Composite Structures 252 (2020) 112702

Contents lists available at ScienceDirect

Composite Structures

journal homepage: www.elsevier.com/locate/compstruct

A novel method to predict the stiffness evolution of in-service wind turbine blades based on deep learning models

Hongwei Liu [a], Zhichun Zhang [a], Hongbo Jia [a], Quanlong Li [b], Yanju Liu [c], Jinsong Leng [a,*]

[a] Center for Composite Materials and Structures, No. 2 Yikuang Street, Science Park of Harbin Institute of Technology (HIT), P.O. Box 301, Harbin, PR China
[b] School of Computer Science and Technology, Harbin Institute of Technology, Harbin 150001, PR China
[c] Department of Astronautical Science and Mechanics, Harbin Institute of Technology, Harbin 150001, PR China

ARTICLE INFO

Keywords:
Deep learning
Wind turbine blade
Fatigue test
Stiffness prediction

ABSTRACT

Since wind turbines operate in a complex environment for long term, the fatigue behavior of the blades can be influenced by wind, illumination, moisture, temperature, and so forth. For wind turbine blade manufacturers, the determination of their fatigue limit before delivery is necessary and fatigue acceleration experiments usually require a lot of labor and experimental costs. As a machine learning paradigm, deep learning focuses on the inherent hierarchical models of data and has achieved notable success in computer vision, speech recognition, natural language processing, etc. Aimed at reducing the time and the costs during fatigue tests, this paper studies a training-based method for wind turbine blade stiffness prediction using time series stiffness data under fatigue tests. Based on deep learning methods including convolutional neural network, long-short term memory network and the hybrid network, the residual stiffness of the blade with fatigue life under fatigue tests is obtained by combining the fatigue historical data. The obtained results show that the developed models can learn features directly from raw stiffness data and complete the residual stiffness prediction in succession. White Gaussian noise with different signal-to-noise ratios is also added to all stiffness data to demonstrate the models' feasibility of stiffness prediction.

1. Introduction

As a kind of renewable and clean energy, wind energy has been a critical factor to solve the fossil fuel problem in the last decades [1,2]. In the growing prosperity field of wind power, as the size and complexity of wind turbine blades increase, the performance of blades, especially the offshore wind turbine blades, should be carefully considered to enable the blades to withstand extreme loads and fatigue. Since the fatigue performance of blades is hard to be obtained by purely theoretical calculation and it is also impossible to directly refer to the existing engineering experience or knowledge from other industries, a full-scale fatigue test method of blades has been adopted to effectively verify whether the blades can meet the design requirements for twenty-year service in advance [3–5]. For wind turbine blades, the high cycle fatigue test is vital in blade qualification before delivery to avoid the catastrophic failures, which will consume huge manpower, material resources and time [6,7].

Blade fatigue tests are generally carried out in accordance with the standards [3], and the damage conditions are usually evaluated by manual observation [8], strain sensors [9], or displacement sensors [10]. All these methods require a complete fatigue in-situ testing process. Proper fatigue damage evolution model is the foundation to predict the fatigue life of composites in engineering applications and is vital for accurate prediction. Residual strength and residual stiffness are often regarded as the characteristic parameters to quantitatively characterize the damage state of composites and they both gradually degrade with time [11]. Based on residual strength, the load spectrum of the fatigue process can be obtained [12,13].

Compared with residual strength, residual stiffness can be measured without affecting the functionality of components and is more suitable for continuously monitoring and assessing the fatigue damage under service, especially for large composite structures [14–16]. The general process and stiffness change of fatigue damage development of composites is roughly illustrated in Fig. 1. Besides, strain and displacement data can be converted to the stiffness of blades during fatigue tests. If early data could be utilized to predict the residual stiffness of the blade in subsequent fatigue tests, the evaluation cost and time would be significantly reduced for blade manufacturers.

The fatigue test process of blade is usually costly and time consuming and brings huge amounts of data. The amount of data being gener-

* Corresponding author.
E-mail address: lengjs@hit.edu.cn (J. Leng).

https://doi.org/10.1016/j.compstruct.2020.112702
Received 1 December 2019; Revised 17 June 2020; Accepted 13 July 2020
Available online 17 July 2020

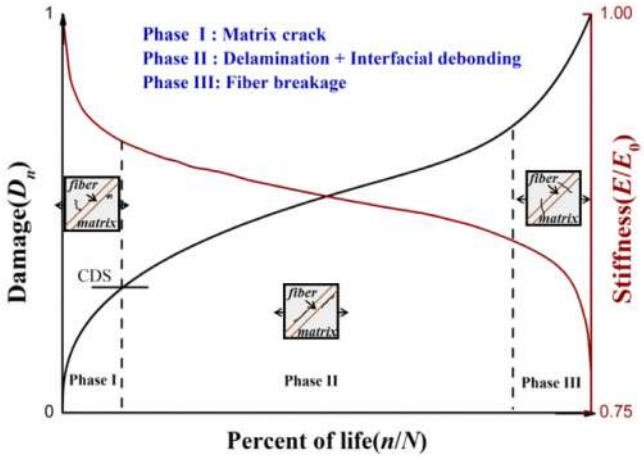

Fig. 1. The nonlinear fatigue damage development of composites.

ated by experiments and simulations has given rise to the fourth paradigm of science over the last few years, which is big data driven science and it is increasingly becoming popular in all fields. Big data brings about the discovery of new materials and new ways of solving problems [17]. Machine learning approaches have gained increasing interests in fault diagnosis and health condition monitoring. They can imitate the mechanism of human learning and realize the analysis of a large number of complex data so as to solve various practical problems.

Machine learning methods and artificial neural networks are adopted for signal processing progressively. By using historical data to train models, machine learning methods can be used for damage identification, classification, and prediction [18]. Xu [19] proposed a complete set of methods, including the clustering analysis, the time-domain analysis, and the spectral analysis, to deal with the acoustic emission signals of bonded composite joints. Qi [20] proposed a mechanical property prediction method of carbon fiber composites based on machine learning, in which the relationship between the properties of carbon fiber monofilaments and the macroscopic parameters of composites was established by a regression tree method. Based on a feed-forward deep neural network (DNN), Liu [21] also gave an initial failure strength prediction of woven composites through a yarn failure criterion. Hu [22] presented a vibration signal processing method of wind turbine blades based on support vector machine (SVM), in which geometric features associated with structural characteristics of impact signals were extracted from both raw vibration signals and energy distribution graph.

With the continuous improvement of computer performance and the gradual maturity of artificial intelligence, the deep model represented by deep training structure emerges, and many researchers applied deep learning models to process data, especially time series data [23]. Deep learning focuses on the inherent hierarchical models of data with less human intervention. In 2014, Takashi [24] firstly used a deep belief network (DBN) consisting of multiple restricted Boltzmann machines (RBM) for time series forecasting. Zhang [25] established a multi-period wind speed prediction model through DBN that demonstrated DBN model provided better predictions purely using wind speed data compared with other models. Dalto [26] combined the variable selection algorithm and DBN to present an ultra-short-term wind prediction model. Wan [27] also proposed a wind speed prediction method based on DBN. Compared with various shallow layer networks, the consequences of the DBN network had a better prediction accuracy.

However, the training time is too long for DBN because of the layer-by-layer training procedure of the network. To reduce the training time and training parameters, a convolutional neural network (CNN) is conducted with its global sharing features. The most outstanding advantage of CNN is that it can automatically learn features from the original images without manual selection, and realize image classification and recognition by adjusting and optimizing the parameters of the convolution kernels through training [28]. However, the CNN model is mainly widely applied in the field of image and video processing, and the input is mostly two-dimensional data. To process one-dimensional time series data using CNN models, one appropriate method is to convert the input time series into a two-dimensional form and then convert the output two-dimensional data into one-dimensional data, which has been realized by Wang et al. [29–31]. Although the conversion may achieve the expected results, the complexity of the model is greatly increased and the prediction accuracy is also affected by the conversion approach. In addition, the two-dimensional data can be converted by wavelet transform or time–frequency transform, by which the obtained wavelet coefficient graph or time–frequency graph is the input of the CNN model. Such methods have been successfully utilized in diagnostic classification [32–35]. However, the aforementioned methods of employing two-dimensional CNN to study the characteristics of time-series signals fail to fully utilize the advantages of the automatic learning of deep learning methods. Considering the temporal relation between data, a long short-term memory (LSTM) model emerges. It is a kind of time recurrent neural network (RNN) and suitable for dealing with the problems concerning time series data [36,37], like speech recognition.

Here, we present a stiffness prediction method considering time series stiffness data under fatigue tests based on CNN and LSTM networks. A hybrid model (CNN-LSTM) is introduced into the task of this stiffness prediction. Due to the difficulty to obtain the stiffness at any time, the stiffness data are obtained from the fatigue calibration tests combining Wu's stiffness degradation model, and the influence of ambient temperature is converted into the change of stiffness. Taking the historical time series data of the same blade type as training data and test data, the variation of the residual stiffness of the blade with fatigue life can be obtained. White Gaussian noise with different signal-to-noise ratios is also added to enhance the universality of stiffness data.

2. Methodology

2.1. Convolutional neural networks

As a specialized network for processing grid-like topology, CNN has been successfully applied in the fields of image and video processing. The network mainly includes convolutional layers, pooling layers and fully connected layers [38]. Among the layers, convolution is the key step of CNN. In convolutional layers, the feature map of an input layer interacts with a convolution kernel or multiple convolution kernels through the convolution method to form an output. Each output feature may also be calculated by the convolution of multiple input feature maps [39]. The convolutional layer output feature map can be expressed as,

$$h_j^l = f\left(\sum_{n=1}^{N}\left(W_{jn}^l * h_n^{l-1}\right) + b^l\right) \tag{1}$$

where the subscript j is the jth convolution kernel, namely the jth output feature map, N is the number of input feature maps, h_j^l is the j th output feature map in the lth layer, h_n^{l-1} is the nth output feature map in the $(l-1)$th layer, namely the input feature map in the lth layer, W_{jn}^l is the nth sub-convolution kernel matrix of the jth convolution kernel, and b^l is the bias for the lth layer. $f(\cdot)$ is the activation function to increase the non-linearity of networks. The convolutional process is

illustrated in Fig. 2. The most common activation functions in machine learning are listed in Table 1. Here, ReLu is adopted and formulated as,

$$f(x) = \max\{x, 0\} \tag{2}$$

It can be seen from the Eq. (1) that the weights of the same output feature map are shared to effectively reduce the computer memory occupancy rate and to improve the computation efficiency. In addition, ReLu function has also been proved to be capable of creating a sparse representation and has a better performance than *sigmoid* function.

Furthermore, the pooling layers are connected to the convolutional layers, which reduce the size of feature maps to control overfitting. The input feature map of a pooling layer is firstly divided into a set of non-overlapping sub-regions through a filter, and then a down-sampling function is used to convert each sub-region into a more concise representation by,

$$h_j^l = f\left(\beta_j^l \cdot down\left(h_j^{l-1}\right) + c_j^l\right) \tag{3}$$

The down-sampling functions include average-pooling and max-pooling, and are respectively expressed by,

$$down\left(h_j^{l-1}\right) = \frac{\sum_{i=1}^{Height}\sum_{j=1}^{Width}\sum_{k=1}^{Length} x_{i,j,k}}{N_L} \tag{4}$$

$$down\left(h_j^{l-1}\right) = \max\left(\sum_{i=1}^{Height}\sum_{j=1}^{Width}\sum_{k=1}^{Length} x_{i,j,k}\right) \tag{5}$$

Fig. 3 shows a diagram of a single depth 4 × 4element processing with a 2 × 2 filter and a 3 × 3 filter through max-pooling and average-pooling. Max-pooling mainly concentrates on feature selection and highlights the characteristic features. While the background information or the baseline will be retained by average-pooling. Here, we used max-pooling Eq. (5). A generalized structure of CNN is also shown in Fig. 4.

2.2. Long short-term memory networks

LSTM is capable of learning long-range connections. Introduced by Hochreiter and Schmidhuber [40], this network eliminates the problems of gradient explosion and gradient disappearance that exist in RNN training models, and has more generalization and better performance than gated recurrent unit (GRU) model. The structure of an

Table 1
Common activation functions in machine learning.

Function name	Function expression	Function characteristics
Sigmoid	$\sigma(x) = 1/(1+e^{-x})$	Easily to cause gradient vanishing problem
Tanh	$\tanh(x) = (e^x - e^{-x})/(e^x + e^{-x})$	Solve the problem 'the Sigmoid output center is not zero', but also easy to cause gradient vanishing problem
ReLu	$\mathrm{ReLu}(x) = \max\{0, x\} = \begin{cases} x & x \geqslant 0 \\ 0 & x < 0 \end{cases}$	Simple, fast and avoids the gradient vanishing problem, but causes 'dead ReLu'
Leaky ReLu	$\mathrm{LeakyReLu}(x) = \begin{cases} x & x \geqslant 0 \\ ax & x < 0 \end{cases}$	Solve the 'dead ReLu' problem
ELU	$\mathrm{ELU}(x) = \begin{cases} x & x \geqslant 0 \\ a \cdot [\exp(x) - 1] & x < 0 \end{cases}$	Solve the 'dead ReLu' problem and the output mean is close to zero, but low efficiency
Softmax	$\sigma(z_j) = \frac{e^{z_j}}{\sum_{k=1}^{n} e^{z_k}}$ for $j = 1, \ldots, n$	Deal with multiple classification problems

LSTM memory cell at each timestep t includes an input gate, a forget gate and an output gate, as illustrated in Fig. 5 [41],

$$\textit{Input gate} \quad \mathbf{i}_t = \sigma(\mathbf{W}_{ix}\mathbf{x}_t + \mathbf{W}_{ia}\mathbf{a}_{t-1} + b_i) \tag{6}$$

$$\textit{Forget gate} \quad \mathbf{f}_t = \sigma\left(\mathbf{W}_{fx}\mathbf{x}_t + \mathbf{W}_{fa}\mathbf{a}_{t-1} + b_f\right) \tag{7}$$

$$\textit{Output gate} \quad \mathbf{o}_t = \sigma(\mathbf{W}_{ox}\mathbf{x}_t + \mathbf{W}_{oa}\mathbf{a}_{t-1} + b_o) \tag{8}$$

$$\tilde{\mathbf{c}}_t = \tanh(\mathbf{W}_{\tilde{c}x}\mathbf{x}_t + \mathbf{W}_{\tilde{c}a}\mathbf{a}_{t-1} + b_{\tilde{c}}) \tag{9}$$

$$\mathbf{c}_t = \mathbf{f}_t * \mathbf{c}_{t-1} + \mathbf{i}_t * \tilde{\mathbf{c}}_t \tag{10}$$

$$\mathbf{a}_t = \mathbf{o}_t * \tanh(\mathbf{c}_t) \tag{11}$$

where $\mathbf{W}_{ix}$, $\mathbf{W}_{ia}$, $\mathbf{W}_{fx}$, $\mathbf{W}_{fa}$, $\mathbf{W}_{ox}$, $\mathbf{W}_{oa}$, $\mathbf{W}_{\tilde{c}x}$ and $\mathbf{W}_{\tilde{c}a}$ represent the gate weight matrices, and b_i, b_f, b_o and $b_{\tilde{c}}$ represent the gate bias vectors. The three gates ($\mathbf{i}_t$, $\mathbf{f}_t$, $\mathbf{o}_t$), representing vectors for the activation values, need to adjust themselves to get an appropriate cell state $\mathbf{c}_t$. $\mathbf{x}_t$ and $\mathbf{a}_t$ are the current LSTM input and output at timestep t, $\mathbf{a}_{t-1}$ and $\mathbf{c}_{t-1}$ stand for the LSTM output and the cell state of the previous time $t-1$. σ stands for *sigmoid* activation function and $\tilde{\mathbf{c}}_t$ stands for the candidate values. Symbol $*$ denotes the Hadamard (elementwise) product.

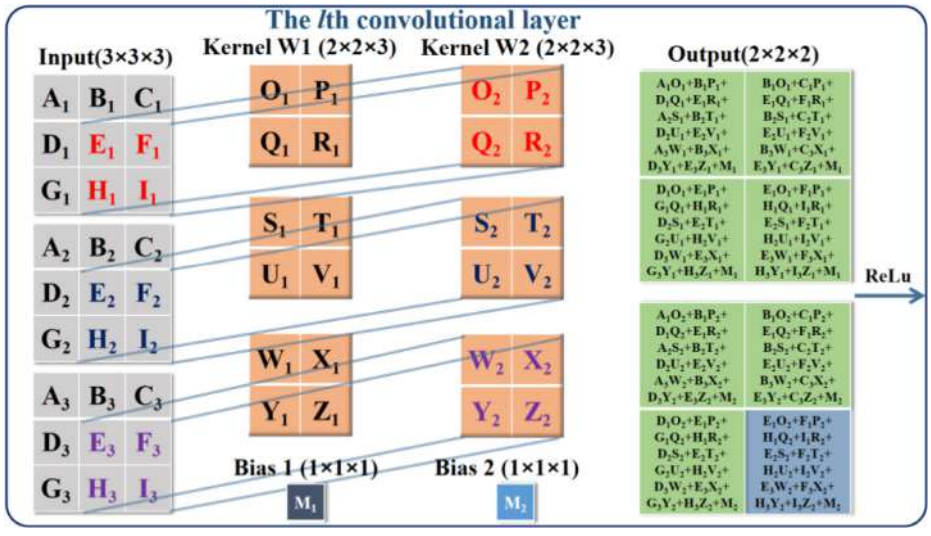

Fig. 2. The convolutional process.

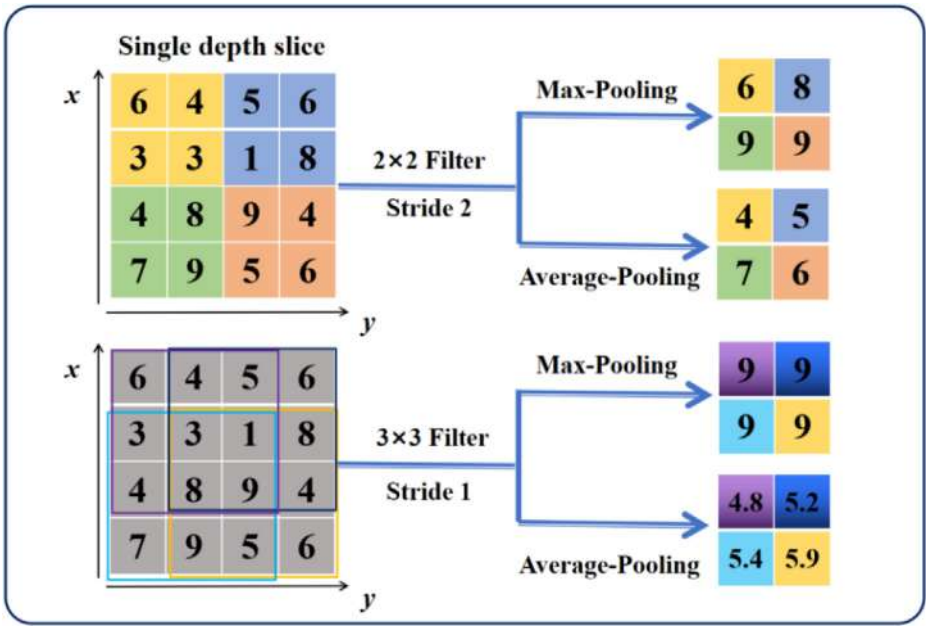

Fig. 3. A diagram of max-pooling and average-pooling with filters.

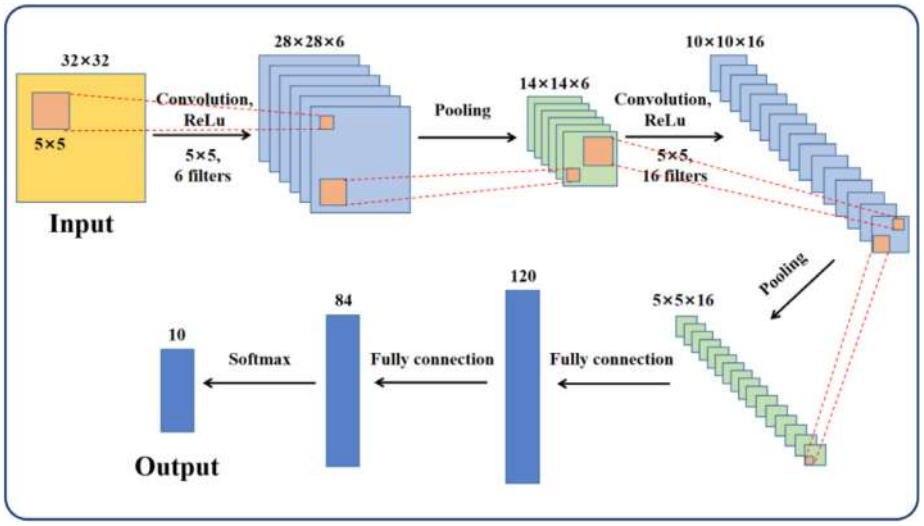

Fig. 4. A generalized schematic diagram of the convolutional neural network.

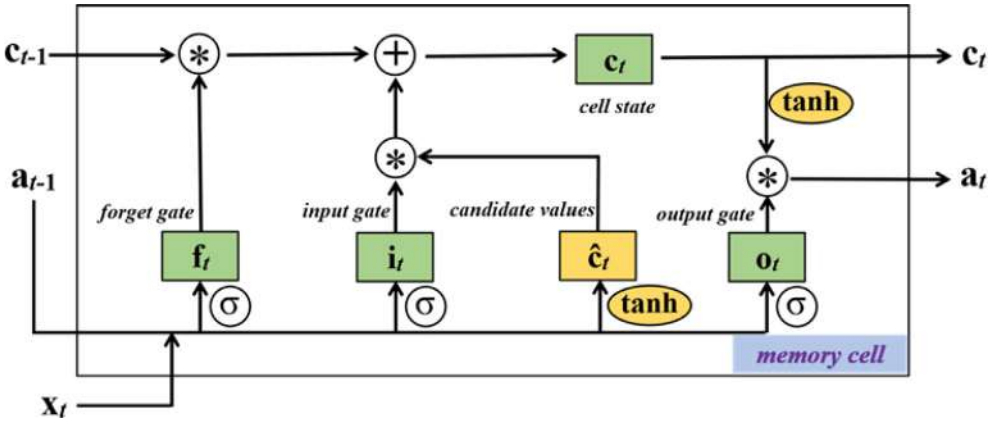

Fig. 5. The schematic diagram of an LSTM memory cell.

When processing time-series input, the features are rendered in the LSTM network time by time. The gates serve as filters for the cell state, fulfilling the information discard, addition, and output. According to Eqs. (6)–(11), the input is processed by the network. Once the last element of the sequence is processed, the final output is returned. Finally, the output $\mathbf{a}_t$ can be converted to the predicted output $\tilde{\mathbf{y}}_t$, expressed as,

$$\tilde{\mathbf{y}}_t = \mathbf{W}_t \mathbf{a}_t \tag{12}$$

where $\mathbf{W}_t$ is a matrix to reduce the dimension of $\mathbf{a}_t$.

2.3. Performance assessment

In the training process, stochastic gradient descent (SGD) is utilized as the loss of the objective function. We used loss functions, including mean square error (MSE), mean absolute error (MAE), root mean square error (RMSE) and mean absolute percentage error (MAPE), as listed in Table 2, for time series prediction.

MAPE and RMSE metrics are chosen to assess the prediction performance.

3. Case study and results

In fatigue tests, the blade stiffness is required to be no less than 90% of initial value to satisfy the design criteria for the equivalent 20 years' fatigue life through 2 million vibration tests. According to the stiffness requirement of blade fatigue tests, we focused on the fatigue test data.

In this section, the feasibility of stiffness prediction based on deep learning methods in the fatigue test was verified through the blade fatigue tests with composite fatigue stiffness degradation model. The influence of different deep learning network structures and input sequences on prediction accuracy was studied. The structures included CNN, LSTM network and the hybrid (CNN-LSTM) network.

3.1. Data pre-processing

The fatigue test data were obtained through blade fatigue tests, as shown in Fig. 6. Depending on the test rule [3,42], adopting the scheme of uniaxial constant stress loading, the blade was fixed transversely on the fatigue test bench through the flange bolts. Calibration tests were conducted by the side-pull equipment and tension sensors during and after the fatigue test to obtain the stiffness changes of the dangerous section. If the stiffness change was lower than 10% and there was no obvious damage, crack, and partial blade instability, it was considered that the blade met the design requirements. The analysis of such anisotropic composite materials in wind turbine blades is relatively complicated. For simplicity, the blade is regarded as a cantilever beam with isotropic material properties under constant loading, and the stiffness can be expressed as,

$$E = \frac{F}{L} \tag{13}$$

Fig. 6. The wind turbine blade fatigue test.

where E is the blade static stiffness, F is the concentrated calibration loading of the blade, L is the measured displacement of the dangerous section. In fact, the change of displacement directly reflects the change of stiffness under the same loading F.

Based on the previous work of Kou [43], a concentrated load was applied to a 52.5 m glass fiber reinforced plastic (GFRP) wind turbine blade (commercial product of Sinoma Wind Power Blade Co. Ltd) for loading calibration. Some of the parameters of the blade are listed in Table 3. Rigorous finite element analysis was performed before the fatigue test of the blade to determine the critical section, and the sensors were attached at several key locations of the blade during fatigue tests. This calibration test was performed 6 times and at the location of 42 m from the root. The measured displacement of the dangerous section was recorded. According to the experience and this 2.5 MW blade structural design, 32 m was the most dangerous point and this position was chosen as an example for stiffness prediction.

The ambient temperature and humidity affect the stiffness during the fatigue test. To take the influence of temperature and humidity into consideration, simultaneous training of stiffness, temperature and humidity will be required. According to Bai's work [44], the stiffness change can reflect the influence of temperature and humidity after treatment. Therefore, using the stiffness is sufficient to evaluate the fatigue of the wind turbine blade. In this way, the complexity of the training network can be reduced, and the depth of the network can be increased conveniently, resulting in better results.

Table 2
Common loss functions.

Function name	Evaluation indexes
MSE	$MSE = \frac{1}{n}\sum_{t=1}^{n}\left(y_t - \tilde{y}_t\right)^2$
MAE	$MAE = \frac{1}{n}\sum_{t=1}^{N}\left\|y_t - \tilde{y}_t\right\|$
RMSE	$RMSE = \sqrt{\frac{1}{n}\sum_{t=1}^{N}\left(y_t - \tilde{y}_t\right)^2}$
MAPE	$MAPE = \frac{100\%}{n}\sum_{t=1}^{n}\left\|\frac{y_t - \tilde{y}_t}{y_t}\right\|$

Table 3
Parameters of the tested turbine blade.

Name	Value
Power	2.5 MW
Blade length	52.2 m
The length of the blade root	2.4 m
Blade mass	10968 kg
maximum chord length	3 m
Position of maximum chord length	3.8 m from the blade root
Airfoil	DU/NACA
rated speed	23 rpm
Main material	Glass fiber reinforced epoxy resin

Table 4
The measured blade stiffness of different fatigue life cycle ratios.

Loading level	Percent of life (n/N)					
	0	0.145	0.250	0.315	0.750	1
20%	1	0.9887	0.9847	0.9821	0.9729	0.9568
40%	1	0.9829	0.9800	0.9781	0.9675	0.9526
60%	1	0.9831	0.9795	0.9779	0.9649	0.9488
80%	1	0.9830	0.9891	0.9767	0.9628	0.9470
100%	1	0.9826	0.9788	0.9771	0.9616	0.9421

Table 5
The bladed damage index of different fatigue life cycle ratios.

Loading level	Percent of life (n/N)					
	0	0.145	0.250	0.315	0.750	1
20%	0	0.26157	0.35417	0.41435	0.62731	1
40%	0	0.36076	0.42194	0.46203	0.68565	1
60%	0	0.33008	0.40039	0.43164	0.68555	1
80%	0	0.32075	0.20566	0.43962	0.70189	1
100%	0	0.30052	0.36615	0.39551	0.66321	1

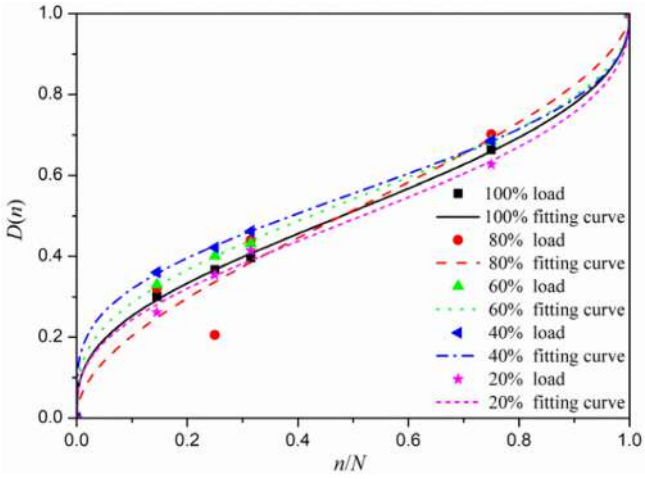

Fig. 7. The damage development curves under different loadings.

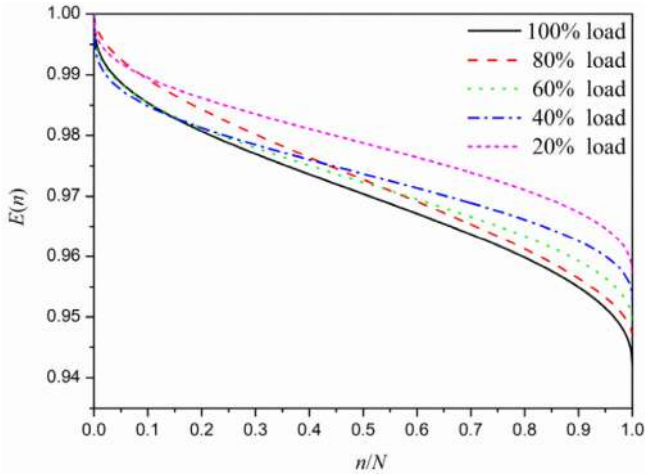

Fig. 8. The stiffness degradation curves under different loadings.

Table 4 shows the measured stiffness after different calibration loadings and fatigue life cycle ratios. According to Wu's stiffness degradation model of composites [45], the damage index can be described as,

$$D(n) = \frac{E_0 - E_n}{E_0 - E_f} = 1 - \left[1 - \left(\frac{n}{N}\right)^b\right]^a \tag{14}$$

where E_0 is the original Young's modulus, E_f is the failure Young's modulus, E_n is the Young's modulus undergoing the nth cyclic loading, n is the corresponding cycle number, N is the fatigue life, and a and b are the material parameters that are fitted from test results. $D(n)$ represents the fatigue damage index, with $D(0) = 0$ indicating the undamaged state and $D(N) = 1$ indicating the fully damaged state. By Eq. (4), the stiffness data in Table 3 are converted into the damage index and listed in Table 5.

Coupled with Wu's stiffness degradation model, the fitting curves of different fatigue life cycle ratios under different loadings are plotted in Fig. 7. And then, the stiffness degradation models under different loading levels can be formulated as,

$$D_{20\%}(n) = 1 - \left[1 - \left(\frac{n}{N}\right)^{0.30605}\right]^{0.40864} \tag{15}$$

$$D_{40\%}(n) = 1 - \left[1 - \left(\frac{n}{N}\right)^{0.21575}\right]^{0.4105} \tag{16}$$

$$D_{60\%}(n) = 1 - \left[1 - \left(\frac{n}{N}\right)^{0.2778}\right]^{0.44747} \tag{17}$$

$$D_{80\%}(n) = 1 - \left[1 - \left(\frac{n}{N}\right)^{0.48915}\right]^{0.57912} \tag{18}$$

$$D_{100\%}(n) = 1 - \left[1 - \left(\frac{n}{N}\right)^{0.31582}\right]^{0.44042} \tag{19}$$

where $D_{20\%}(n)$, $D_{40\%}(n)$, $D_{60\%}(n)$, $D_{80\%}(n)$ and $D_{100\%}(n)$ stand for the damage index corresponding to different fatigue life cycles under the loading level of 20%, 40%, 60%, 80%, 100%, respectively. Substituting the Eqs. (15)–(19) into the Eq. (14), the stiffness of different fatigue life cycle ratios can be obtained as follows,

$$E_{20\%}(n) = 0.9568 \times \left\{1 - \left[1 - \left(\frac{n}{N}\right)^{0.30605}\right]^{0.40864}\right\} + \left[1 - \left(\frac{n}{N}\right)^{0.30605}\right]^{0.40864} \tag{20}$$

$$E_{40\%}(n) = 0.9526\times\left\{1-\left[1-\left(\frac{n}{N}\right)^{0.21575}\right]^{0.4105}\right\} + \left[1-\left(\frac{n}{N}\right)^{0.21575}\right]^{0.4105} \quad (21)$$

$$E_{60\%}(n) = 0.9488\times\left\{1-\left[1-\left(\frac{n}{N}\right)^{0.2778}\right]^{0.44747}\right\} + \left[1-\left(\frac{n}{N}\right)^{0.2778}\right]^{0.44747} \quad (22)$$

$$E_{80\%}(n) = 0.9470\times\left\{1-\left[1-\left(\frac{n}{N}\right)^{0.48915}\right]^{0.57912}\right\} + \left[1-\left(\frac{n}{N}\right)^{0.48915}\right]^{0.57912} \quad (23)$$

$$E_{100\%}(n) = 0.9421\times\left\{1-\left[1-\left(\frac{n}{N}\right)^{0.31582}\right]^{0.44042}\right\} + \left[1-\left(\frac{n}{N}\right)^{0.31582}\right]^{0.44042} \quad (24)$$

where $E_{20\%}(n)$, $E_{40\%}(n)$, $E_{60\%}(n)$, $E_{80\%}(n)$ and $E_{100\%}(n)$ stand for the stiffness of blades after different fatigue life cycles under the loading level of 20%, 40%, 60%, 80%, 100%, respectively. Fig. 8 plots the stiffness degradation curves based on the experimental data of the blade under different loadings.

Here, Wu's stiffness degradation model is chosen just to expand the data set. Since Wu's model is a general model for composites, the calibrated data are fitted to the model to obtain the engineering stiffness model formula of the blade, thus obtaining a large number of data points.

Since the stiffness data measured by the calibration experiment are limited and deep learning methods rely on abundant sample data sets, the stiffness degradation curve data are treated as training data and test data to verify the feasibility of this stiffness prediction method.

In the following study, all proposed training network models are implemented using Keras and executed on Nvidia GeForce GTX 1070. GPU has powerful computing ability and memory bandwidth and the usage of GPU instead of CPU to train certain fatigue loading tests and evaluation can reduce plenty of computing time.

Since the feature value range of the original data varies in a wide range, data normalization is particularly important, especially when multiple features are compared. Voluminous data normalization methods can be employed, such as normalization, mean normalization, standardization. Here, normalization is used to scale the feature range in [0, 1], and expressed as

$$x' = \frac{x - \min(X)}{\max(X) - \min(X)} \quad (25)$$

where x represents an original value of X, x' represents the corresponding normalized value of X.

The stiffness data organization strategy is depicted in Fig. 9. All stiffness data are available from the stiffness degradation curves. For example, 1000 stiffness data can be acquired from a single stiffness degradation curve. Taking the aggregate of 5000 stiffness data from the five curves into consideration, the total data are separated into 90% training data and 10% test data. In addition, 15% of the training data act as the validation set.

The losses of the training set and verification set are reduced gradually through back propagation method to optimize the training network during the training process. The input series is the anterior m

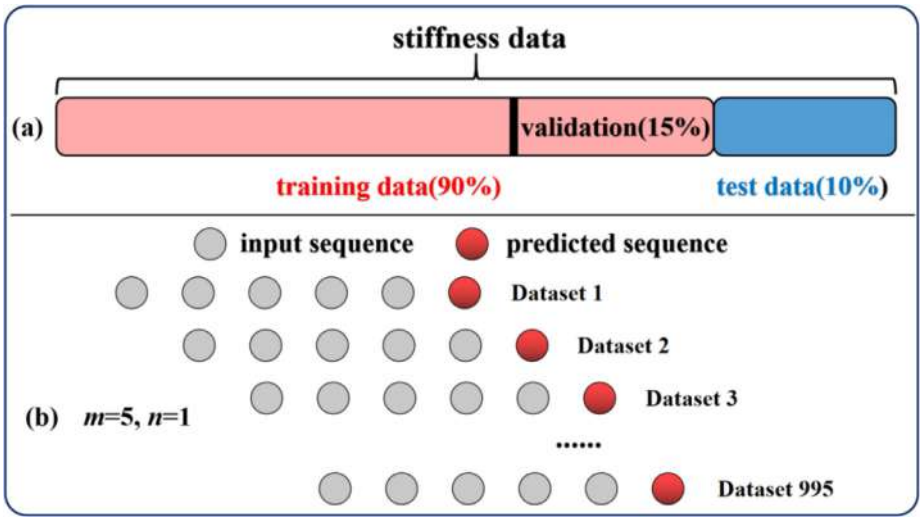

Fig. 9. The stiffness data organization strategy.

Table 6
MAPE and RMSE for different models and sequence lengths.

Number of neurons	Sequence length = batch size					
	m = 1		m = 5		m = 10	
	MAPE (%)	RMSE	MAPE (%)	RMSE	MAPE (%)	RMSE
16	0.032	0.00040	0.061	0.00065	0.035	0.00055
32	0.036	0.00042	0.018	0.00027	0.057	0.00070
64	0.030	0.00035	0.032	0.00045	0.133	0.00155
128	0.049	0.00056	0.019	0.00021	0.069	0.00079
128 + 16	0.124	0.00133	0.018	0.00020	1.042	0.01136
64 + 8	0.192	0.00210	0.054	0.00060	0.059	0.00061

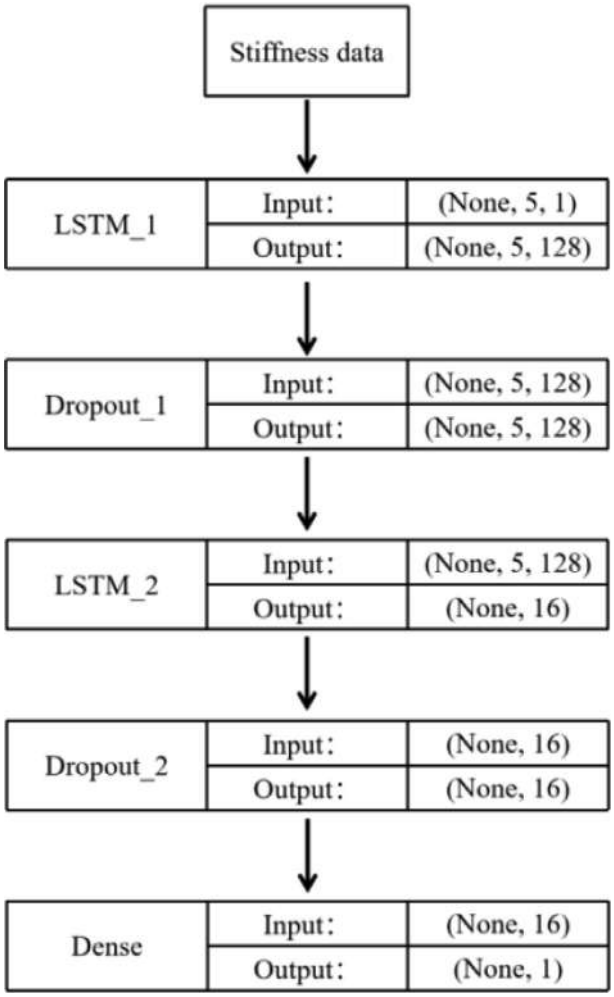

Fig. 10. Double LSTM layers model structure diagram.

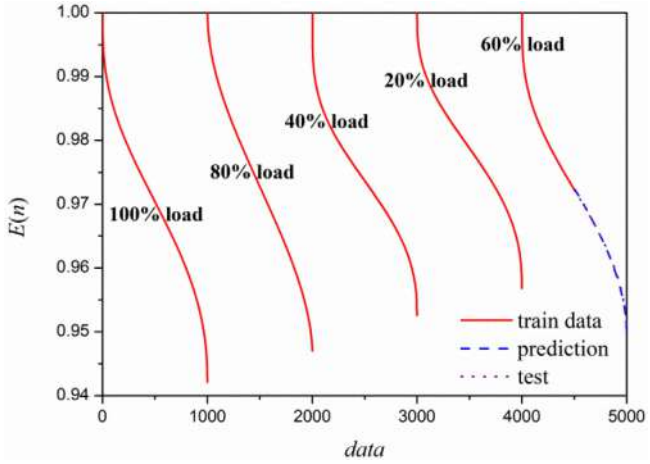

Fig. 11. The prediction results of the stiffness data based on the LSTM model.

samples (sequence length) and the output prediction series is the following n predicted samples. According to Qin's work [46], the performance of the network will be declined with the growth of forecast prospect in most cases. So making n much smaller is beneficial for network training and prediction. It can be observed in Fig. 8 (b), 1000 data have been changed into 995 datasets when $m = 5$, $n = 1$.

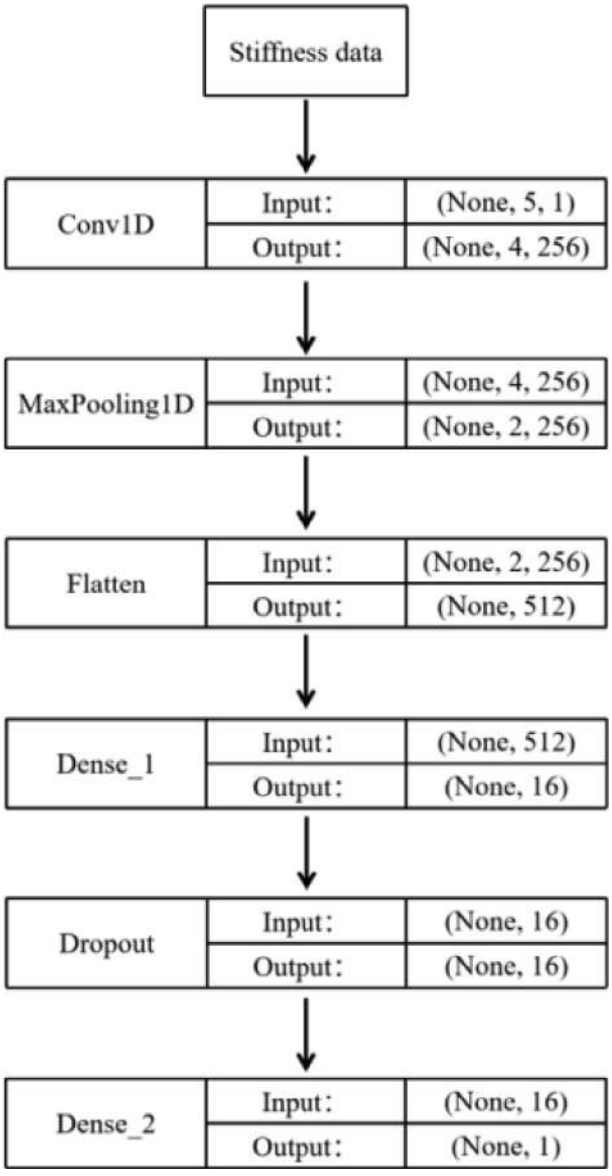

Fig. 12. An optimized CNN model structure diagram.

In the test process, the test set is made available for the trained network and the predicted results are obtained according to the training model. The training network is assessed by comparing the difference between the forecast values and the actual values of the test set.

3.2. Training and evaluating LSTM models

In this section, different models based on LSTM are trained and evaluated combining the stiffness data. The stiffness data are divided as shown in Fig. 9(a) and the stiffness data of 100% load, 80% load, 40% load, 20% load, half of 60% load are treated as training data (4500 data points). The data of the other half of 60% load are treated as test data (500 data points).

To train the models, an Adam optimization operator (learning rate = 0.0001, decay = 0.001) is adopted, and the models are learned with minimization of MSE (loss function) by back propagation method. The optimization operator and loss function of Sections 3.3 and 3.4 are the same. As to evaluate, the efficiency is tested with MAPE and RMSE metrics. The dropout value is set as 0.5 to prevent gradient disappearance and gradient explosion as well as to achieve excellent performance during the training process. The effect on the

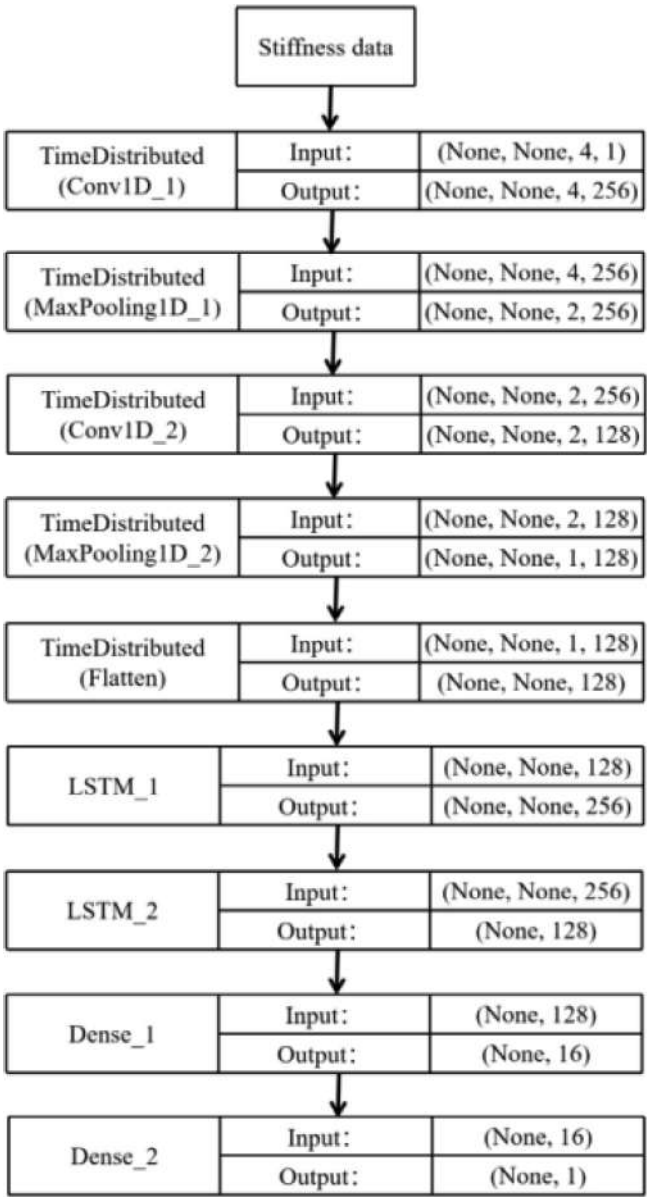

Fig. 13. The CNN-LSTM hybrid model structure diagram.

number of neurons and the number of network layers (1 or 2) on the prediction results are compared under various sequence lengths. MAPE and RMSE results for different LSTM models with different sequence lengths are listed in Table 6.

Smaller MAPE and RMSE values indicate the higher accuracy of the prediction models. For different sequence lengths, different LSTM models have separate evaluation results. It can be seen in Table 6, the sequence length m = 5 is better than m = 1, which is too short to truly reflect the trend of the curve, or m = 10, which is too long to show the trend obviously. Fig. 10 shows the most optimized LSTM structure diagram (128 + 16, m = 5) with double LSTM layers in Table 6. Based on the double LSTM layers model, the prediction stiffness data compared with training data and test data are shown in Fig. 11.

3.3. Training and evaluating CNN models

To maximize the close connection between the stiffness data, one dimensional CNN is adopted. The input is purely the raw stiffness data without signal processing, and would not cause the degradation of model performance due to the human factors. Besides, the training set, test set, optimization operator and loss function of CNN models are exactly the same as LSTM models. Different CNN models are further studied, but not listed below for simplicity.

Fig. 12 shows an optimized CNN structure diagram, of which MAPE (%) is 0.0348 and RMSE is 0.00041. Compared with the double LSTM layers model, it has been demonstrated that the prediction of the stiffness data can also be achieved successfully. But the CNN model's performance is slightly worse, mainly due to the lack of correlation among data.

3.4. Training and evaluating CNN-LSTM models

Aimed at combining the benefits of CNN and LSTM, a novel hybrid model (CNN-LSTM) is proposed for blade stiffness prediction. Here, the CNN part contains two convolutional layers with the kernel number of 256, 128 and two max-pooling layers. Two LSTM layers with 256 and 128 neurons and two fully connected layers are also adopted in the hybrid model. The aggregate model structure is shown in Fig. 13. The MAPE (%) result of the CNN-LSTM model is 0.0047 and the RMSE consequence is 0.00008. It shows that the model has a good performance.

Furthermore, the consequences of different proposed models in this paper are listed in Table 7. Among all the models, the MAE, RMSE and MAPE values of the CNN-LSTM model are smaller than those of the single model (LSTM, CNN), indicating that the hybrid model can generate better prediction results. Larger R^2 can result in better prediction.

Based on the training data and the proposed models, the subsequent results can be predicted. It is clear to show the predicted results in Fig. 14. The predicted results have the same tendency as the test data and the CNN-LSTM model matches better.

3.5. Enhanced data set and the training model

According to the previous discussion, the data of stiffness degradation curves are used to generate training data and test data to verify the feasibility of this stiffness prediction method. In fact, due to the errors from the test instruments and sensors, the measured values are not completely consistent with the stiffness degradation curves and have fluctuations. In order to verify the universality of data set selection and reflect the advantages of deep learning methods, white Gaussian noise with different signal-to-noise ratio (SNR) is added to all stiffness degradation data.

Based on the CNN-LSTM model, the predicted results of the stiffness data with different SNR are compared in Table 8. With the increase of SNR and the reduction of the noise signal, the prediction results can be more accurate.

The predicted results of the stiffness data with SNR at 65 dB and 75 dB are shown in Fig. 15 as examples to verify the generality of data set selection. The predicted results of the CNN-LSTM model have the same tendency with the test data although with slight fluctuation. In

Table 7
The prediction results of different deep learning models.

Models	Results			
	MAE	RMSE	MAPE (%)	R^2
LSTM	0.00017	0.00020	0.018	0.9987
CNN	0.00033	0.00041	0.035	0.9942
CNN-LSTM	**0.00006**	**0.00008**	**0.0047**	**0.9997**

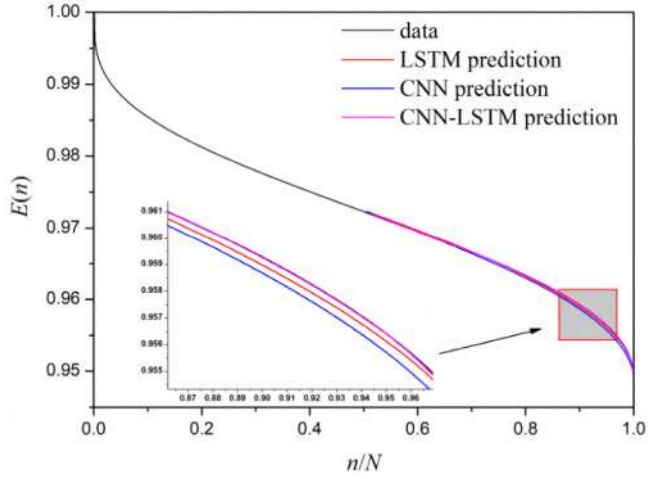

Fig. 14. The prediction results of different proposed models (a) data with 65 dB noise (b) data with 75 dB noise.

fact, when the obtained time series data fluctuates greatly, some denoising methods can be used for data denoising.

3.6. Accuracy of the predictions under different training sets

In this section, different training sets and test sets based on CNN-LSTM are trained and evaluated combining the stiffness data.

Case1: The stiffness data of 80% load, 60% load, 40% load, 20% load, half of 100% load are treated as training data (4500 data points). The data of the other half of 100% load are treated as test data (500 data points).

Case2: The stiffness data of 100% load, 60% load, 40% load, 20% load, half of 80% load are treated as training data (4500 data points). The data of the other half of 80% load are treated as test data (500 data points).

Case3: The stiffness data of 100% load, 80% load, 40% load, 20% load, half of 60% load are treated as training data (4500 data points). The data of the other half of 60% load are treated as test data (500 data points).

Case4: The stiffness data of 100% load, 80% load, 60% load, 20% load, half of 40% load are treated as training data (4500 data points). The data of the other half of 40% load are treated as test data (500 data points).

Case5: The stiffness data of 100% load, 80% load, 60% load, 40% load, half of 20% load are treated as training data (4500 data points). The data of the other half of 20% load are treated as test data (500 data points).

The results of different cases are listed in Table 9. The prediction results obtained under different sets prove the feasibility and robustness of this method.

Table 8
The prediction results of the stiffness data with different SNR.

SNR (dB)	Results			
	MAE	RMSE	MAPE (%)	R^2
65	0.00047	0.00060	0.049	0.9872
70	0.00031	0.00040	0.033	0.9942
75	0.00017	0.00026	0.019	0.9976
80	0.00016	0.00021	0.017	0.9983

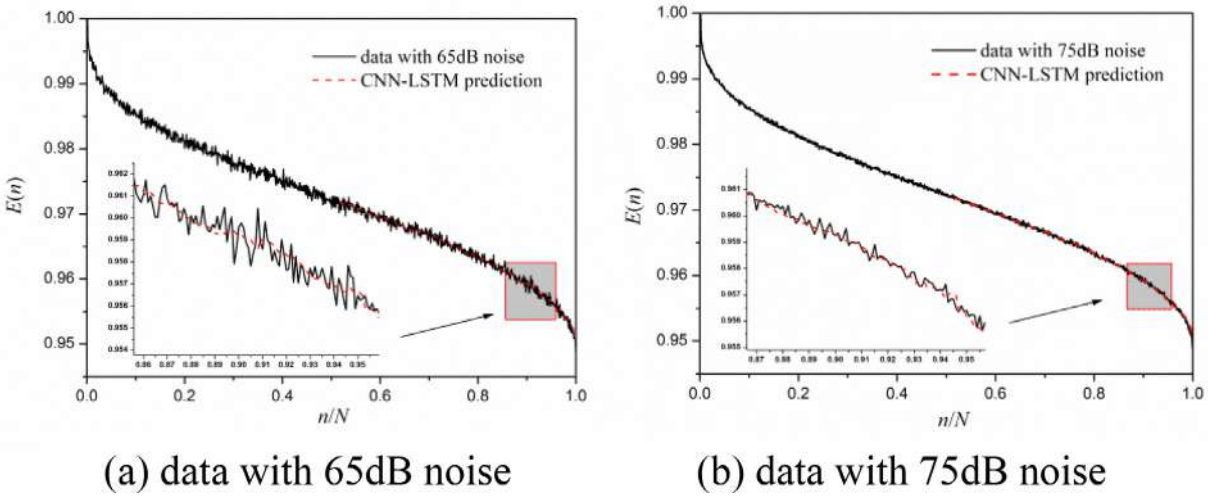

Fig. 15. The prediction results of the stiffness data with SNR at 65 dB and 75 dB.

Table 9
The prediction results of different data sets with CNN-LSTM model.

Case	Results			
	MAE	RMSE	MAPE (%)	R^2
Case1	0.00011	0.00013	0.0067	0.9991
Case2	0.00008	0.00012	0.0059	0.9993
Case3	0.00006	0.00008	0.0047	0.9997
Case4	0.00012	0.00014	0.0070	0.9990
Case5	0.000007	0.00011	0.0053	0.9995

4. Conclusions

In this paper, a wind turbine blade stiffness prediction method based on the deep learning networks is proposed. Three types of training models (CNN, LSTM, CNN-LSTM) are applicable to realize this effective prediction considering the historical fatigue stiffness data. Various input sequence lengths are conducted to show the effectiveness of our models. The prediction results prove that the models can learn features directly from raw stiffness data and well predict the residual stiffness.

Three types of training models (CNN, LSTM, CNN-LSTM) are also compared and evaluated. The prediction performance of the CNN-LSTM model is preferable when compared to that of a single model (CNN, LSTM) under the uniform data set. Combining the advantages of different network models, these models can be connected together to surmount the weakness of a single network. The CNN units are usually used to get the spatial features, and the LSTM units are to get the connection among series data. Therefore, the predictive performance of the CNN-LSTM model is better.

White Gaussian noise with different signal-to-noise ratio (SNR) is added to all stiffness data to verify the universality of data set selection. The prediction results of the CNN-LSTM model are slightly different from the test data, but the overall trend is completely consistent, due to the random noise. Five cases of different data sets are also studied in this paper. The predicted results are close to the test results and the method is proved to be feasible. Better predictions can be obtained by increasing the diversity of training data samples.

Combining the deep learning methods, the subsequent stiffness evolution of a blade can be predicted through learning the empirical mode from the sample base, which is established based on the historic stiffness change data from previous blade fatigue tests, and the early test data. Thus the cost for evaluating newly fabricated blades can be significantly reduced.

CRediT authorship contribution statement

Hongwei Liu: Conceptualization, Investigation, Visualization, Writing - original draft, Writing - review & editing. **Zhichun Zhang:** Methodology, Supervision, Data curation, Writing - review & editing. **Hongbo Jia:** Visualization, Investigation, Writing - review & editing. **Quanlong Li:** Investigation, Writing - review & editing. **Yanju Liu:** Visualization, Writing - review & editing. **Jinsong Leng:** Conceptualization, Methodology, Investigation, Writing - review & editing.

Declaration of Competing Interest

The authors declare that they have no known competing financial interests or personal relationships that could have appeared to influence the work reported in this paper.

Acknowledgement

This work is supported by the Foundation for Innovative Research Groups of the National Nature Science Foundation of China (Grant No. 11421091) and Special Funds for Scientific and Technological Innovation Talents of Harbin (Grant No. JJ20170379). The authors also thank Dr. Ming Lei from Northwestern Polytechnical University and Jinrong Li from Harbin Institute of Technology for their kind help.

References

[1] REN 21 Steering Committee. Renewables 2018 global status report. Report, Renewable Energy Policy Network for the 21st Century; 2018. Paris, France: REN21 Secretariat.
[2] REN 21 Steering Committee. Renewables 2019 global status report. Report, Renewable Energy Policy Network for the 21st Century; 2019. Paris, France: REN21 Secretariat.
[3] International Electrotechnical Commission. IEC TS 61400-23 Wind turbine generator systems-part 23: full-scale structural testing of rotor blades. Switzerland: International Electrotechnical Commission; 2014
[4] Lee HG, Park J. Static test until structural collapse after fatigue testing of a full-scale wind turbine blade. Compos Struct 2016;136:251–7.
[5] Su HM, Kam TY. Reliability analysis of composite wind turbine blades considering material degradation of blades. Compos Struct 2020;234:111663.
[6] Othman AK, Homayoun H, Christian L, Gavin G, Peter G, Kirsten D. Full-scale fatigue testing of a wind turbine blade in flapwise direction and examining the effect of crack propagation on the blade performance. Materials 2017;10:1152.
[7] Lee HG, Lee J. Measurement theory of test bending moments for resonance-type fatigue testing of a full-scale wind turbine blade. Compos Struct 2018;200:306–12.
[8] Chen X. Experimental observation of fatigue degradation in a composite wind turbine blade. Compos Struct 2019;212:547–51.
[9] Tian SH, Yang ZB, Chen XF, Xie Y. Damage detection based on static strain responses using FBG in a wind turbine blade. Sensors 2015;15(8):19992–20005.
[10] Gao F, Wu XJ, Liu Q, Liu JC, Yang XY. Fault simulation and online diagnosis of blade damage of large-scale wind turbines. Energies 2019;12:522.
[11] Sevenois RDB, Van PW. Fatigue damage modeling techniques for textile composites: review and comparison with unidirectional composite modeling techniques. Appl Mech Rev 2015;67(2):021401.
[12] Epaarachchi JA, Clausen PD. The development of a fatigue loading spectrum for small wind turbine blades. J Wind Eng Ind Aerod 2006;94(4):207–23.
[13] Epaarachchi JA, Clausen PD. An empirical model for fatigue behavior prediction of glass fibre-reinforced plastic composites for various stress ratios and test frequencies. Compos Part A 2003;34(4):313–26.
[14] Highsmith AL, Reifsnider KL. Stiffness-reduction mechanisms in composite laminates, damage in composite materials. ASTM STP 1982;775:103–17.
[15] Whitworth HA. Modeling stiffness reduction of graphite/epoxy composite laminates. J Compos Mater 1987;21(4):362–72.
[16] Mao H, Mahadevan S. Fatigue damage modeling of composite materials. Compos Struct 2002;58:405–10.
[17] Agrawal A, Choudhary A. Perspective: materials informatics and big data: realization of the “fourth paradigm” of science in materials science. APL Mater 2016;4(5):053208.
[18] Jordan MI, Mitchell TM. Machine learning: Trends, perspectives, and prospects. Science 2015;349:6245.
[19] Xu D, Liu PF, Li JG, Chen ZP. Damage mode identification of adhesive composite joints under hygrothermal environment using acoustic emission and machine learning. Compos Struct 2019;211:351–63.
[20] Qi ZC, Zhang NX, Liu Y, Chen WL. Prediction of mechanical properties of carbon fiber based on cross-scale FEM and machine learning. Compos Struct 2019;212:199–206.
[21] Liu X, Gasco F, Goodsell J, Yu WB. Initial failure strength prediction of woven composites using a new yarn failure criterion constructed by deep learning. Compos Struct 2019;230:111505.
[22] Hu CC, Albertani R. Machine learning applied to wind turbine blades impact detection. Wind Eng 2019;1:1–14.
[23] Romeu P, Zamor MF, Botella RP, Pardo J. Time-series forecasting of indoor temperature using pre-trained deep neural networks. International conference on artificial neural networks, 2013.
[24] Takashi K, Shinsuke K, Kunikazu K, Masanao O. Time series forecasting using a deep belief network with restricted Boltzmann machines. Neurocomputing 2014;137:47–56.
[25] Zhang CY, Chen CLP, Gan M, Chen L. Predictive deep Boltzmann machine for multiperiod wind speed forecasting. IEEE T Sustain Energ 2015;6(4):1416–25.
[26] Dalto M, Matusko J, Vasak M. In: Deep neural networks for ultra-short-term wind forecasting. IEEE; 2015. p. 1657–63.

[27] Wan J, Liu JF, Ren GR, Guo YF, Hu QH. Day-ahead prediction of wind speed with deep feature learning. Int J Pattern Recognit Artif Intell 2016;30(05):1650011.
[28] Lee KB, Cheon S, Kim CO. A convolutional neural network for fault classification and diagnosis in semiconductor manufacturing processes. IEEE Trans Semiconduct Manuf 2017;30(2):135–42.
[29] Wang HZ, Yi HY, Peng JC, Wang GB, Liu YT, Jiang H, et al. Deterministic and probabilistic forecasting of photovoltaic power based on deep convolutional neural network. Energ Convers Manage 2017;153:409–22.
[30] Sezer OB, Ozbayoglu AM. Algorithmic financial trading with deep convolutional neural networks: time series to image conversion approach. Appl Soft Comput 2018;70:525–38.
[31] Wang HZ, Li GQ, Wang GB, Peng JC, Jiang H, Liu YT. Deep learning based ensemble approach for probabilistic wind power forecasting. Appl Energ 2017;188:56–70.
[32] Han T, Yuan JH, Tang J, An LZ. An approach of intelligent compound fault diagnosis of rolling bearing based on MWT and CNN. J Mech Transmiss 2016;40 (12):139–43.
[33] Yuan JH, Han T, Tang J, An LZ. An approach to intelligent fault diagnosis of rolling bearing using wavelet time-frequency representations and CNN. Mach Des Res 2016;33(2):93–7.
[34] Sun WF, Yao B, Zeng NY, Chen BQ, He YC, Cao XC, et al. An intelligent gear fault diagnosis methodology using a complex wavelet enhanced convolutional neural network. Materials 2017;10(7):790.
[35] Jing LY, Zhao M, Li P, Xu XQ. A convolutional neural network based feature learning and fault diagnosis method for the condition monitoring of gearbox. Measurement 2017;111:1–10.
[36] Qing XY, Niu YG. Hourly day-ahead solar irradiance prediction using weather forecasts by LSTM. Energy 2018;148:461–8.
[37] He W. Load forecasting via deep neural networks. Procedia Comput Sci 2017;122:308–14.
[38] Zeiler MD, Fergus R. Visualizing and understanding convolutional neural networks. European conference on computer vision. 2013
[39] Wu LY, Cheng JZ, Li SL, Lei BY, Wang TF, Ni D. FUIQA: fetal ultrasound image quality assessment with deep convolutional networks. IEEE Trans Cybern 2017;47 (5):1336–49.
[40] Hochreiter S, Schmidhuber J. Long short-term memory. Neural Comput 1997;9 (8):1735–80.
[41] Fischer T, Krauss C. Deep learning with long-term memory networks for financial market predictions. Eur J Oper Res 2018;270(2):654–69.
[42] General Administration of Quality Supervision, Inspection and Quarantine of the People's Republic of China. Turbine blade of wind turbine generator system full-scale structural testing of rotor blades. 2010; GB/T 25384
[43] Kou HX. Research on stiffness degradation model of composite wind turbine blades. [Doctoral Dissertation]. China: Lanzhou University of Technology; 2019
[44] Bai X, An Z, Hou Y, Ma Q. Health assessment and management of wind turbine blade based on the fatigue test data. Microelectron Reliab 2017;75:205–14.
[45] Wu FW, Yao WX. A fatigue damage model of composite materials. Int J Fatigue 2010;32(1):134–8.
[46] Qin Y, Li K, Liang ZH, Lee B, Zhang FY, Gu YC, et al. Hybrid forecasting model based on long short term memory network and deep learning neural network for wind signal. Appl Energ 2019;236:262–72.